

# Super-efficient temporal solitons in mutually coupled optical microresonators

Xiaoxiao Xue\*, Xiaoping Zheng, and Bingkun Zhou

*Department of Electronic Engineering, Beijing National Research Center for Information Science and Technology,  
Tsinghua University, Beijing 100084, China*

[\\*xuexx@tsinghua.edu.cn](mailto:xuexx@tsinghua.edu.cn)

## Abstract

Optical frequency combs are one of the most important tools in a broad spectrum of applications. Recently, microresonator based optical frequency comb (microcomb) generation has emerged as a revolutionary technology which shows the merits of chip-level integration, high repetition rate, and ultrabroad bandwidth. Temporal cavity solitons have attracted intense interest because they correspond to low-noise and broadband mode-locked combs in the frequency domain. However, the application of soliton microcombs is fundamentally limited in many cases by the low energy conversion efficiency. Here we propose a strategy of breaking this limitation with mutually coupled microresonators by mimicking impedance matching in radiofrequency electronics. We derive a new set of coupled nonlinear Schrödinger equations with a precise full map to model the soliton dynamics. Numerical computations show tens-to-hundreds-of-fold improvement of the energy conversion efficiency for single-soliton microcomb generation. The super-efficient microcomb source will benefit a wide range of applications for which the conversion efficiency is crucial.

An optical frequency comb is a coherent laser source which contains a series of phase locked and equally spaced oscillating frequencies. Optical frequency combs have served as one of the most important tools in a broad spectrum of applications ranging from fundamental science to high-speed telecommunications [1]-[4]. Recently, optical microresonator based frequency comb (usually named microcomb or Kerr comb) generation has been investigated intensely [5]-[7]. Such highly compact and chip-level integrated comb sources may revolutionize many applications which can previously only be maintained inside laboratories due to their large volume and high power consumption [8]-[14].

The basic scheme of microcomb generation is composed of a passive nonlinear microresonator coherently pumped by a continuous-wave (c.w.) laser. In the frequency domain, the comb generation is explained by cascaded four-wave mixing which transfers the energy from the pump to newly generated frequency lines. In the time domain, the comb mode locking is generally related to formation of temporal solitons in the cavity [15], [16]. Due to the high quality (Q) factor of the microresonator, the pump field can be greatly enhanced in the cavity with coherent build-up. Significant nonlinear processes are then attainable with very little input power. Pumping threshold in the mW and sub-mW level for comb initiation has been demonstrated with various microresonator platforms [17]-[22]. Nevertheless, achieving high energy conversion efficiency, which is defined as the ratio of the pump power converted to the other frequency lines, has proved to be one fundamental challenge for microcombs [23]. The conversion efficiency is cru-

cial for many practical applications. For example, in wavelength-division multiplexed fiber telecommunications, the power of each comb line is closely related to the signal-to-noise ratio at the receiver and thus determines the achievable spectral efficiency and transmission distance [24]. Since the solitons are highly localized in time, the energy conversion is confined in a very limited time window [25]. The efficiency of bright soliton combs generated with anomalous-dispersion microresonators is typically only a few percent ( $<1\%$  in many cases) [26]. And the shorter the soliton pulse width (corresponding to more comb lines in spectrum) is, the poorer the conversion efficiency results. The conversion efficiency may be improved by maintaining multiple solitons in the cavity [27], [28], but at the price of reducing the number of comb lines and introducing large variations in the comb spectrum. Another way to increase the efficiency is by using a pulsed laser pump whose repetition rate is synchronized to that of the cavity soliton [29]-[31]. But the basic limitation still exists, namely larger spectral broadening ratio in comb generation corresponds to lower conversion efficiency. Dark soliton combs in the normal-dispersion region have attracted a lot of interest due to their larger duty cycle and correspondingly higher efficiency [16], [25], [32], [33]. However, dark soliton combs usually have narrower spectra compared to bright solitons. And further improvement of the efficiency proves to be extremely challenging.

In this article, we show that efficient conversion of the pump power to the comb lines can be achieved by coupled-mode frequency matching with a configuration of mutually coupled optical microresonators. Using coupled nonlinear Schrödinger equations with a full map and rigorous numerical computations, we demonstrate soliton microcombs with extraordinarily high energy conversion efficiency. Soliton excitation strategies including single-shot pulse trigger and spontaneous excitation from chaos are also investigated.

## Coupled-mode frequency matching for efficient energy transfer

Before introducing the proposed concept, it is instructive to rethink why the conversion efficiency of soliton microcombs is limited. It has been proved both theoretically and experimentally that bright temporal solitons exist in an effectively red-detuned region (i.e. the frequency (wavelength) of the pump laser field is lower (longer) than the resonant frequency (wavelength) of the microresonator) [15]. This pump-resonator frequency detuning is critical to maintain the solitons but at the same time prevents the pump power efficiently entering the microresonator. A prerequisite of high conversion efficiency is significant reduction of the pump power after interacting with the microresonator. However, most soliton microcombs show spectra with high contrast between the pump and the comb lines, implying very poor energy conversion efficiency. The problem can simply be explained by the resonant conditions illustration in Fig. 1. When the pump frequency matches that of the resonator (MR1) and the coupling rate equals the decay rate (Fig. 1a, case I), the pump power from port P can be completely transferred to the drop channel (port D) – a condition usually called critical coupling. Here the meaning of the drop channel is generalized which may account for intrinsic losses, coupling loss related to a drop waveguide, and nonlinear losses in case of comb generation. However, when the pump frequency is not equal to the resonant frequency, complete power transfer is not possible (Fig. 1a, case II). But if there is another resonator (denoted as MR2) coupled with MR1 and the input field (for simplicity, MR2 is assumed intrinsically lossless), full power transfer to the drop channel of MR1 can be achieved when the follow-

ing condition is satisfied (Fig. 1a, case III; see Supplementary Section 1 for the mathematic details).

$$\kappa_P = \frac{|\kappa_C|^2 \kappa_D}{(\omega_P - \omega_1)^2 + \kappa_D^2} \quad (1)$$

$$\omega_2 = \omega_P - \frac{|\kappa_C|^2 (\omega_P - \omega_1)}{(\omega_P - \omega_1)^2 + \kappa_D^2} \quad (2)$$

where  $\omega_1$ ,  $\omega_2$ , and  $\omega_P$  are the angular frequencies of resonator MR1, MR2, and the pump field;  $\kappa_D$  is the coupling rate between MR1 and the drop channel;  $\kappa_C$  is the coupling rate between MR1 and MR2;  $\kappa_P$  is the coupling rate between MR2 and the pump field.

We note that such a method of using coupled modes to maximize energy transfer can find its analogs in impedance matching in radiofrequency electronics [34]. Inspired by this insight, we propose a configuration of mutually coupled microresonators for high-efficiency microcomb generation. As illustrated in Fig. 1b, when the device is operating, a single temporal soliton is formed in MR1 while MR2 acts as a frequency adapter which matches the pump to MR1 to maximize energy conversion. The soliton comb is extracted from a drop port of MR1. At the through port of MR1, the pump field is ideally significantly degraded due to the efficient power transfer to the comb. The nonlinearity of MR2 is not necessary in principle, but since both microresonators are most likely fabricated with the same material, we will thus consider all their nonlinearities in the next.

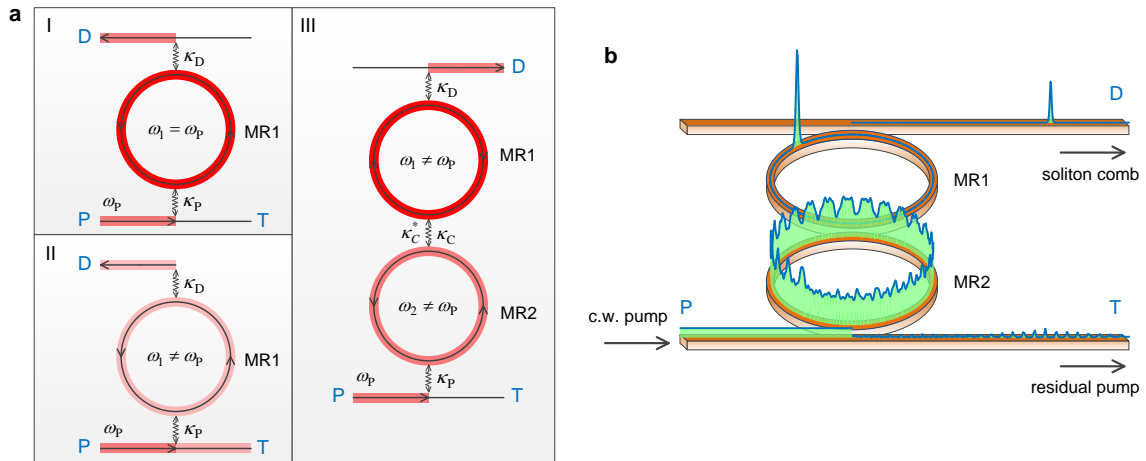


Figure 1 | Efficient energy transfer with coupled modes. **(a)**. Case I: when the pump frequency matches the resonator (MR1) frequency ( $\omega_1 = \omega_P$ ) and the coupling rates satisfy  $\kappa_P = \kappa_D$ , all the power from port P can be transferred to port D; case II: when the pump frequency does not match the resonator ( $\omega_1 \neq \omega_P$ ), full power transfer is impossible; case III: when a second microresonator (MR2) is incorporated, full power transfer can be achieved again if its frequency and the coupling rates satisfy Eqs. (1) and (2). **(b)**. Super-efficient temporal soliton comb generation with mutually coupled microresonators. The soliton circulates in MR1, while MR2 acts as a frequency adapter to maximize the power transfer from the pump to the soliton.

## Results

**A case of intrinsically lossless microresonators.** The evolution of the optical fields in MR1 and MR2 can be described by a set of coupled nonlinear Schrödinger equations (see Methods for the details and Supplementary Section 2 for the equation derivation). The key parameters in our numerical computations, such as Kerr nonlinear coefficient and group velocity dispersion, are comparable to the typical values for silicon nitride microring resonators which can be fabricated with a complementary metal–oxide–semiconductor compatible technique [35]. The intrinsic losses due to scattering and material absorption constitute one fundamental energy waste when the light propagates in the microresonator. One continuing effort in microresonator fabrication is thus to reduce the intrinsic losses and increase the intrinsic Q factor. One interesting question is what conversion efficiency we can get if we have ideal microresonators with completely no intrinsic losses (corresponding to infinite intrinsic Q). Note that for traditional comb generation with a single microresonator, the conversion efficiency of bright soliton combs is still quite limited even with an intrinsically lossless microresonator [25]. Here we consider a similar condition for mutually coupled microresonators. A more practical example including the intrinsic losses will be investigated in a later section.

According to the principle explained above, only coupling of the pumped modes between the two microresonators is necessary to facilitate energy transfer. To avoid strong interactions of the other modes which may destroy the soliton [36], slightly different radii are chosen for MR1 and MR2. The free spectral ranges (FSRs) of MR1 and MR2 are 200 GHz and 192.6 GHz, respectively. The group velocity dispersion of MR1 is anomalous ( $-100 \text{ ps}^2/\text{km}$ ) which is necessary to support bright temporal solitons. To reduce the possibility of modulational instability in MR2 which is undesired in our scheme, the dispersion of MR2 is chosen to be normal ( $100 \text{ ps}^2/\text{km}$ ). The different signs of dispersion can easily be achieved by tailoring the waveguide dimensions in fabrication. The pump power injected from port P is 20 mW. The initial optical fields inside the microresonators are given by the steady-state c.w. solutions of the coupled nonlinear Schrödinger equations. A single-shot Gaussian pulse, which has a full-width-at-half-maximum (FWHM) of 0.2 ps and a peak power of 200 W, is introduced in MR1 at a certain time. We carefully adjust the frequency detunings between the pump field and the microresonators to find the solitons (see Methods for a detailed list of all the parameters). The numerical results show that the pulse quickly evolves to a stable temporal soliton with a FWHM of 24 fs in nanoseconds (see Supplementary File I for an animation).

Since strong depletion of the pump power in the bus waveguide is usually a clue of efficient energy conversion, we optimize the device parameters in our simulations to minimize the pump at port T. The optical fields in the microresonators and in the bus waveguides are shown in Fig. 2a. In the bus waveguides, the soliton at port D takes 98.0% of the total input power and the residual power at port T is only 2.0%. The optical field inside MR2 is very close to a c.w. with an average power of 1.9 W. Figure 2b shows the comb spectra in the bus waveguides. At port D, a smooth single-soliton comb can be observed. The conversion efficiency defined as the ratio of the comb power at port D excluding the pump line over the total input pump power is 94.2%. At port T, the pump line is significantly degraded which means the pump is close to effective critical coupling in comb operation. There are periodic comb clusters which are generated due to mode coupling

between the microresonators where their frequencies get close. From MR1's point of view, the situation closely resembles a soliton driven by a c.w. pump field of 1.9 W as in the case of a single microresonator. The soliton spectrum generated by pumping MR1 from MR2 while MR2 is assumed open is also shown in Fig. 2b, which is indeed very close to the soliton spectrum obtained in mutually coupled microresonators. But in the case of single-microresonator comb generation, the energy conversion efficiency is merely 1.0%. The proposed mutually coupled microresonators can thus significantly improve the efficiency. From one point of view, MR2 can be regarded as a pump amplifier that boosts the pump power for MR1 and a coupling adaptor that maintains a close-to-critical-coupling condition for the pump in comb generation.

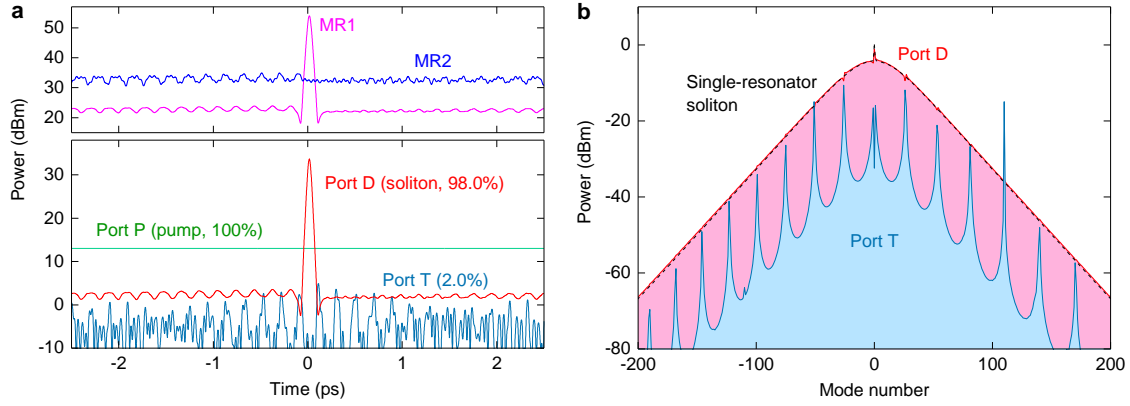


Figure 2 | Soliton solution in mutually coupled microresonators assuming no intrinsic losses. The pump power is 20 mW. **(a)** Time-domain waveforms. Top: in the cavities; bottom: in the bus waveguides. The soliton at port D contains 98.0% of the total power, while the residual power at port T is only 2.0%. **(b)** Comb spectra in the bus waveguides. Significant pump degradation can be observed at port T, corresponding to a high conversion efficiency of 94.2%. The black dash line shows the spectrum of a traditional soliton comb generated with a single microresonator (MR1; also measured at port D) pumped by 1.9 W.

**Spontaneous soliton excitation from chaos.** As demonstrated above, the soliton can be stimulated by a single-shot pulse trigger. Experimentally the trigger pulse can be injected from the opposite side to port D. The required peak power in the bus waveguide is about 22 kW. One potential candidate of the trigger pulse source can be a fiber mode-locked laser. Another way to obtain the soliton is spontaneous excitation with modulational instability as has been widely employed in single-resonator comb generation. To do so, the c.w. pump laser is tuned into the microresonator from the blue side (i.e. pump laser wavelength shorter than the resonant wavelength). In our case of mutually coupled microresonators, one prerequisite of obtaining modulational instability in MR1 is getting enough power build-up in its cavity. Since MR1 is not directly coupled to the pump waveguide, the resonance of MR1 is only visible through its coupling to MR2. To evaluate the power build-up condition, it is helpful to look at the linear transmission of the mutually coupled microresonators.

For the investigations in this section, we consider the intrinsic losses of MR1 and MR2 corresponding to an intrinsic  $Q$  of  $10^7$ . Such  $Q$  levels have been demonstrated with the state-of-the-

art integration techniques [21], [22]. The energy of the soliton circulating in MR1 is dissipated through intrinsic loss and coupling loss. Higher conversion efficiency can be expected if the ratio of the coupling loss over the intrinsic loss is higher. Therefore, we assume MR1 is over-coupled to the drop waveguide corresponding to an external  $Q$  of  $0.5 \times 10^6$ . The power coupling ratio between MR2 and the pump waveguide is optimized for high conversion efficiency and also results in an over-coupling condition. Figure 3a shows the linear transmission of port D and port T. The input probe field is injected from port P. Exact frequency matching is assumed for the modes of MR1 and MR2 which are pumped in comb generation (corresponding to zero frequency in the figure). The modes become hybridized due to coupling of MR1 and MR2. The transmission at port T shows a high extinction ratio close to critical coupling (see the region marked with a dash box). Strong field build-up in MR1 can be observed from the transmission of port D. For the modes other than the pumped, the frequency detuning between MR1 and MR2 gets larger. Their resonances tested at port T tend to the natural transmission of MR2 (i.e. the case of no coupling between MR1 and MR2) and are much weaker (recall that MR2 is over-coupled to the bus waveguide; note that in a frequency range larger than that shown in Fig. 3a, the modes of MR1 and MR2 may become closer again periodically). Therefore, to achieve strong field build-up, the pumped modes of MR1 and MR2 should be close enough in the comb initiation stage. Figure 3b shows zoom-in plots of the pumped mode with different detunings between MR1 and MR2, which is a typical picture of avoided mode crossing. Experimentally measured results as Fig. 3b can be found in [37].

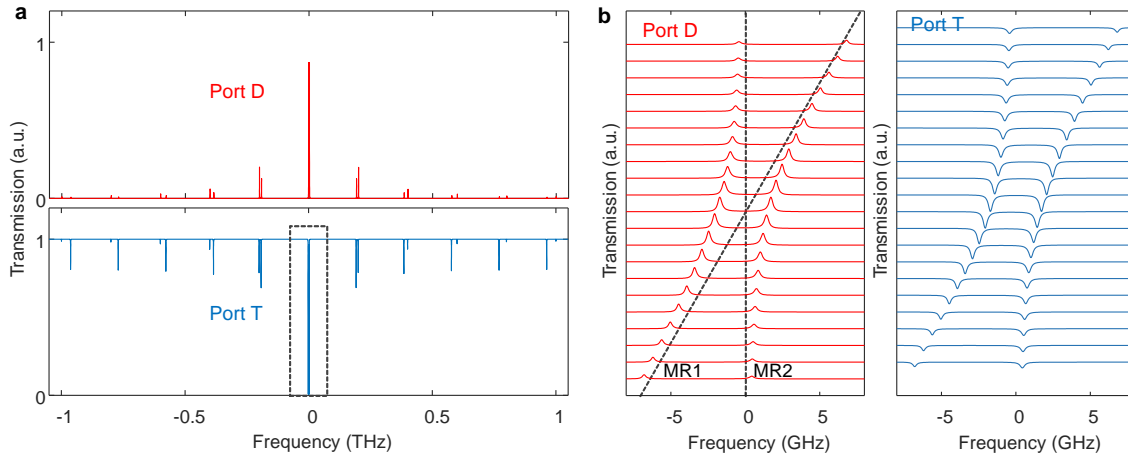
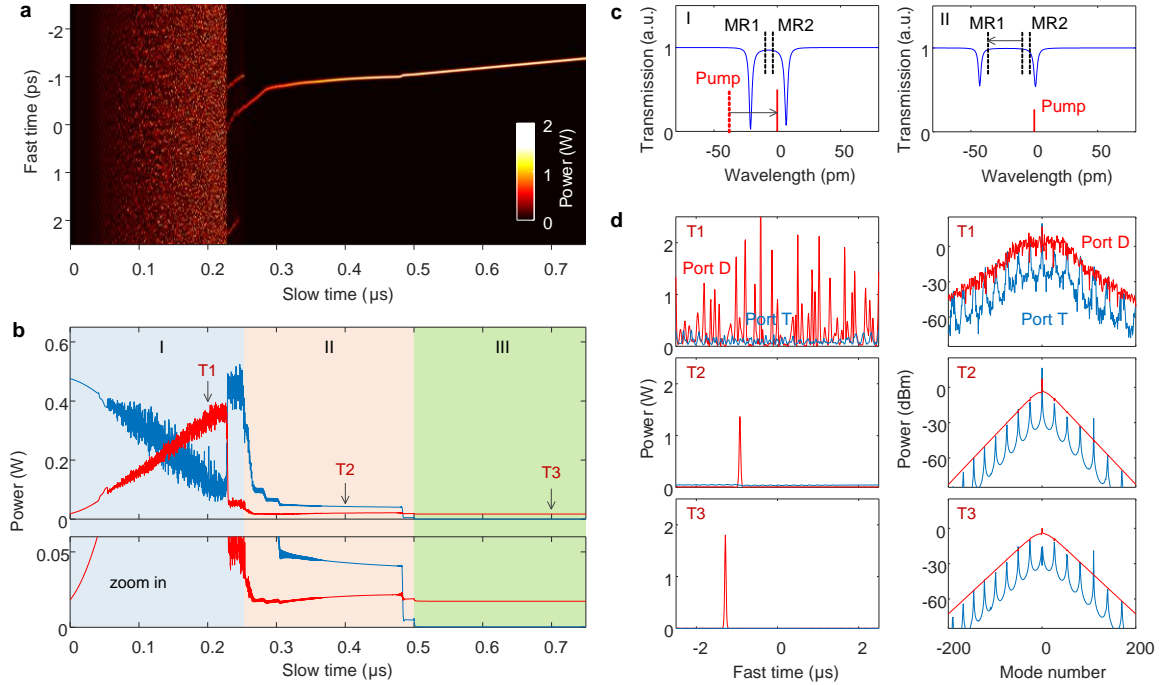


Figure 3 | Linear transmission of mutually coupled microresonators. The probe field is injected from port P. (a) Transmission of drop port (port D) and through port (port T). The modes around zero frequency (marked in a dash box) are pumped in comb generation. The natural frequencies of MR1 and MR2 are assumed equal for the pumped modes. (b) Zoom-in of the pumped modes with different detunings between MR1 and MR2, showing a typical picture of avoided mode crossing. The dash lines indicate the natural resonant frequencies.

Figure 4 shows one example of spontaneous soliton excitation. In stage I, the wavelength of MR1 is slightly red detuned with respect to MR2. The pump laser scans across the resonance from the red side as in usual microcomb generation experiments [15] (see the illustration in Fig.

4c, left). The pump power is 500 mW. The evolution of the optical field in MR1 is shown in Fig. 4a. The power transmission at port T and port D is shown in Fig. 4b. As the pump is tuned into the resonance, modulational instability occurs and frequency combs are generated. The comb then turns to a chaotic state with randomly changing time-domain waveforms. As the pump laser is tuned further, power transition is observed and a single soliton is generated after transition. In stage II, MR1 is tuned to shorter wavelength while the wavelengths of the pump laser and MR2 are fixed (see the illustration in Fig. 4c, right). This corresponds to increasing the detuning between MR1 and the pump. The soliton is compressed and the peak power increases in this process. In the meanwhile, the pump power is reduced adaptively to suppress soliton breathing. In stage III, a stable and high-efficiency single-soliton comb is finally obtained with a pump power of 20 mW. The soliton FWHM is 26 fs. The time-domain waveforms and the comb spectra at different times in the soliton excitation process are shown in Fig. 4d (see Methods for a detailed list of simulation parameters and Supplementary File II for an animation). In stage III, the power from port D and port T is 86.6% and 1.8% respectively. About 11.6% of the input power is lost due to the intrinsic losses. The comb conversion efficiency is 81.6%.



**Figure 4 | Spontaneous soliton excitation from chaos. (a)** Evolution of the time-domain waveform in MR1. The fast time is related to the angular position in the cavity. The slow time is related to the propagation distance. **(b)** Power transmission at port T and port D. In stage I, the pump laser is tuned from shorter wavelength to longer wavelength with a power of 500 mW. A single soliton is obtained in MR1 at the end of laser tuning. In stage II, MR1 is tuned to shorter wavelength, while the wavelengths of the pump laser and MR2 are fixed and the pump power is adaptively reduced to suppress soliton breathing. In stage III, the optical field in MR1 evolves to a stable high-efficiency soliton. The pump power is 20 mW. **(c)** Linear transmission in stage I (left), and at the end of stage II and in stage III (right). The dash lines show the natural frequencies of MR1 and MR2. **(d)** Time-domain waveforms (left) and comb spectra (right) at port T and port D at different times marked in (b).

Interestingly, the coupling of MR1 and MR2 not only enables high comb power conversion efficiency, but also affects the soliton dynamics in MR1. We investigated the repeatability of spontaneous soliton excitation described above, and found that the soliton transition from chaos is more deterministic than in a single microresonator without mode coupling [15]. Figure 5 shows the overlapped power transmission traces at port D, plotted based on the results of 100 numerical tests. The different colors represent different probabilities. About 70% of the tests transition to a single-soliton state while 30% transition to a c.w. state with no solitons. No multi-soliton states are observed. We attribute the more deterministic single-soliton transition to a similar mechanism as in a single microresonator with spatial mode coupling [38] or fundamental-second-harmonic coupling [39]. Moreover, soliton drifting can be observed from Fig. 4a in stage III, which implies a deviation of the soliton repetition rate from the FSR of MR1. The retrieved soliton repetition rate is 200.0013 GHz in comparison to the 200-GHz FSR of MR1. This effect is also attributed to the coupling between MR1 and MR2, and was again observed in a single multi-mode microresonator [39], [40].

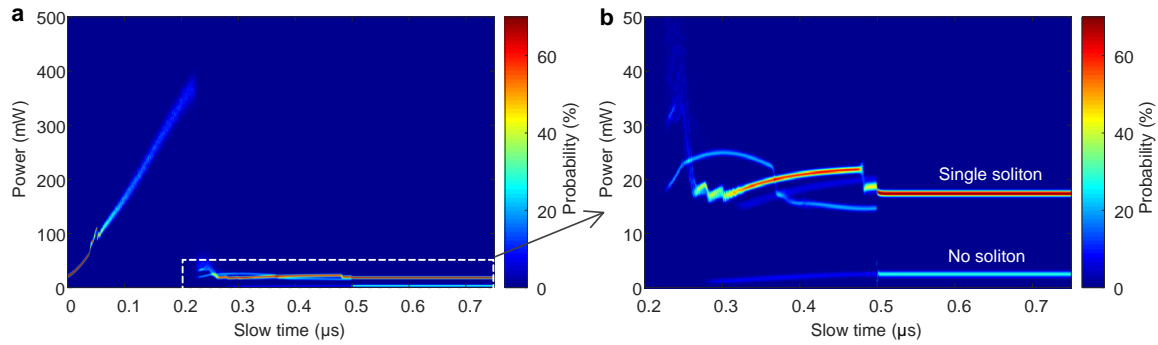


Figure 5 | Repeatability of spontaneous soliton excitation. **(a)** Overlapped power transmission traces at port D. The different colors indicate different probabilities which are calculated based on results of 100 numerical tests. **(b)** Zoom-in of the dash lined region in (a).

## Summary and discussion

In summary, we have proposed and theoretically demonstrated soliton microcomb generation with mutually coupled microresonators to achieve extraordinarily high energy conversion efficiency. The soliton can be excited by a single-shot pulse trigger or spontaneously from chaos with modulational instability. Using parameters comparable to on-chip integrated microresonators, we numerically demonstrate single-soliton comb generation with conversion efficiency higher than 80%. The super-efficient soliton microcomb will benefit a wide range of applications including high-capacity and long-distance fiber telecommunications, biological and chemical sensing, fast detecting lidar, microwave photonic signal processing, etc.

Note that the thermo-optic effect is not considered in our current numerical model. The thermal shifting of microresonator may affect the soliton stability related with power transitions [15], but can be overcome by several technical tricks such as pump laser scanning [15], power kicking [41], and microresonator tuning [27], [42]-[44]. Microresonator tuning is also required in



our scheme to control the frequency detunings between the microresonators and the pump. Depending on different microresonator materials, potential methods may include integrated thermal heaters [42], [43], free-carrier dispersion effect [27], and electro-optic effect [44]. On the other hand, the impact of thermal effect will be reduced by increasing the microresonator intrinsic  $Q$  (i.e. reducing the power absorbed which generates heat).

The coupled nonlinear Schrödinger equations we developed can easily be modified to include higher-order terms such as Raman scattering, higher-order dispersion, and self-steepening. The impact of higher-order terms may become more significant for ultrashort soliton pulses with ultrabroad spectra (e.g. octave-spanning). Since our model is based on a full map, the equations can also be used to model super cavity solitons which exist in a large pump-resonator detuning region where a mean-field approach is no longer valid [45], [46]. Even higher conversion efficiency may be achieved by exploring new soliton states [47].

We note that coupled-microresonator structure was proposed before for tuning the local dispersion as well as the coupling condition [37], [48]. The investigations were not put in the context of high-efficiency temporal solitons and the demonstrated efficiency was still limited to a few percent. No corresponding theoretical model has ever been reported to provide insight into the soliton dynamics before the current contribution. Mutually coupled microresonators provide more freedom of linear and nonlinear mode interactions, and show more rich dynamics than a single microresonator. We expect our proposal and findings will have a wide impact on the microcomb field in both science and technology.

## Methods

The evolution of the optical fields is described by the following coupled nonlinear Schrödinger equations with a full map (see Supplementary Section 2 for equation derivation and more explanations of each symbol).

$$\begin{aligned} \frac{\partial E_1}{\partial z} = & \left[ -\alpha_{11} - i\delta_1 - i\frac{k_1''}{2} \frac{\partial^2}{\partial \tau^2} + i\gamma_1 |E_1|^2 \right] E_1 - \sum_{n=-\infty}^{+\infty} \delta(z-nL) (1-\sqrt{1-\theta_1}) E_1 \\ & + \sum_{n=-\infty}^{+\infty} \delta\left(z-nL-\frac{L}{2}\right) \left[ i\sqrt{\theta_{12}} E_2 - (1-\sqrt{1-\theta_{12}}) E_1 \right] \end{aligned} \quad (3)$$

$$\begin{aligned} \frac{\partial E_2}{\partial z} = & \left[ -\alpha_{12} - i\delta_2 - \Delta k' \frac{\partial}{\partial \tau} - i\frac{k_2''}{2} \frac{\partial^2}{\partial \tau^2} + i\gamma_2 |E_2|^2 \right] E_2 + \sum_{n=-\infty}^{+\infty} \delta(z-nL) \left[ i\sqrt{\theta_2} E_{in} - (1-\sqrt{1-\theta_2}) E_2 \right] \\ & + \sum_{n=-\infty}^{+\infty} \delta\left(z-nL-\frac{L}{2}\right) \left[ i\sqrt{\theta_{21}} E_1 - (1-\sqrt{1-\theta_{21}}) E_2 \right] \end{aligned} \quad (4)$$

$$E_T = i\sqrt{\theta_2} E_2|_{z=nL} + \sqrt{1-\theta_2} E_{in} \quad (5)$$

$$E_D = i\sqrt{\theta_1} E_1|_{z=nL} \quad (6)$$

where  $E_1$ ,  $E_2$ ,  $E_T$ ,  $E_D$  and  $E_{in}$  are complex field amplitudes in MR1, MR2, port T, port D, and port P, normalized so that  $|E_*|^2$  represents the power;  $z$  is the propagation distance in the cavities (the dimension of MR2 is scaled such that the optical field in it shares the same circumferential coordinate as in MR1; see Supplementary Section 2 for more details);  $\alpha_{i1,i2}$  intrinsic amplitude loss per unit length;  $\delta_{i,2}$  phase detunings per unit length;  $\Delta k'$  group velocity mismatch;  $k_{i,2}''$  group velocity dispersion;  $\gamma_{i,2}$  nonlinear coefficients;  $L$  circumference of MR1;  $\theta_1$  power coupling ratio between MR1 and the drop waveguide (port D);  $\theta_2$  power coupling ratio between MR2 and the pump waveguide (port P/T);  $\theta_{12} = \theta_{21}$  power coupling ratio between MR1 and MR2;  $\delta(\bullet)$  the Dirac function.

The equations are numerically integrated with the split-step Fourier method [49]. For the results shown in Fig. 2, the parameters are  $FSR_1 = 200$  GHz (MR1),  $FSR_2 = 192.6$  GHz (MR2),  $L = 1.499$  mm,  $\alpha_{i1} = \alpha_{i2} = 0$ ,  $k_1'' = -100$  ps<sup>2</sup>km<sup>-1</sup>,  $k_2'' = 100$  ps<sup>2</sup>km<sup>-1</sup>,  $\gamma_1 = \gamma_2 = 1$  m<sup>-1</sup>W<sup>-1</sup>,  $\Delta k' = 1.282 \times 10^{-10}$  s·m<sup>-1</sup>,  $\theta_1 = 9.114 \times 10^{-3}$ ,  $\theta_2 = 1.063 \times 10^{-2}$ ,  $\theta_{12} = 3.038 \times 10^{-3}$ ,  $E_{in} = 0.1414$  W<sup>-1/2</sup>,  $\delta_1 = 1.201 \times 10^2$  m<sup>-1</sup>,  $\delta_2 = 8.809$  m<sup>-1</sup>. The corresponding frequency detunings of MR1 ( $\Delta f_1$ ) and MR2 ( $\Delta f_2$ ) with respect to the pump are 5.730 GHz and 0.4048 GHz, respectively. The relation between  $\Delta f_{i,2}$  and  $\delta_{i,2}$  is given by  $\Delta f_{i,2} = FSR_{i,2} \cdot \delta_{i,2} L / (2\pi)$ . For the results shown in Figs. 3, 4, and 5, the parameters are  $FSR_1 = 200$  GHz (MR1),  $FSR_2 = 192.6$  GHz (MR2),  $L = 1.499$  mm,  $\alpha_{i1} = \alpha_{i2} = 0.2027$  m<sup>-1</sup>,  $k_1'' = -100$  ps<sup>2</sup>km<sup>-1</sup>,  $k_2'' = 100$  ps<sup>2</sup>km<sup>-1</sup>,  $\gamma_1 = \gamma_2 = 1$  m<sup>-1</sup>W<sup>-1</sup>,  $\Delta k' = 1.282 \times 10^{-10}$  s·m<sup>-1</sup>,  $\theta_1 = 8.507 \times 10^{-3}$ ,  $\theta_2 = 1.155 \times 10^{-2}$ ,  $\theta_{12} = 3.038 \times 10^{-3}$ . In stage I, the pump power is 500 mW ( $E_{in} = 0.7071$  W<sup>-1/2</sup>); the frequency detunings of MR1 and MR2 with respect to the pump ( $\Delta f_1, \Delta f_2$ ) are synchronously tuned from  $(-1.910$  GHz,  $-2.698$  GHz) to  $(1.273$  GHz,  $0.4852$  GHz) at a speed of 12.73 GHz/ $\mu$ s (equivalent to scanning the pump laser frequency while MR1 and MR2 frequencies are fixed). In stage II, the frequency detuning of MR1 is tuned from 1.273 GHz to 4.775 GHz at a speed of 12.73 GHz/ $\mu$ s and the pump power is adaptively reduced to avoid soliton breathing. In stage III, the frequency detunings of MR1 and MR2 are fixed at 4.775 GHz and 0.4852 GHz, respectively; and the pump power is fixed at 20 mW.

## References

- [1] Udem, T., Holzwarth, R. & Hänsch, T. W. Optical frequency metrology. *Nature* **416**, 233–237 (2002).
- [2] Ye, J., Schnatz, H. & Hollberg, L. W. Optical frequency combs: from frequency metrology to optical phase control. *J. Sel. Top. Quantum Electron.* **9**, 1041–1058 (2003).
- [3] Fortier, T. M. *et al.* Generation of ultrastable microwaves via optical frequency division. *Nat. Photon.* **5**, 425–429 (2011).
- [4] Hillerkuss, D. *et al.* 26 Tbit s<sup>-1</sup> line-rate super-channel transmission utilizing all-optical fast Fourier transform processing. *Nat. Photon.* **5**, 364–371 (2011).
- [5] Kippenberg, T. J., Holzwarth, R. & Diddams, S. A. Microresonator-based optical frequency combs. *Science* **332**, 555–559 (2011).
- [6] Pasquazi, A. *et al.* Micro-Combs: A novel generation of optical sources. *Phys. Rep.* **729**, 1–81 (2018).
- [7] Weiner, A. M. Frequency combs: Cavity solitons come of age. *Nat. Photon.* **11**, 533–535 (2017).

- [8] Liang, W. *et al.* High spectral purity Kerr frequency comb radio frequency photonic oscillator. *Nat. Comm.* **6**, 7957 (2015).
- [9] Suh, M.-G., Yang, Q.-F., Yang, K. Y., Yi, X. & Vahala, K. J. Microresonator soliton dual-comb spectroscopy. *Science* **354**, 600–603 (2016).
- [10] Marin-Palomo, P. *et al.* Microresonator-based solitons for massively parallel coherent optical communications. *Nature* **546**, 274–279 (2017).
- [11] Huang, S.-W. *et al.* Globally Stable Microresonator Turing Pattern Formation for Coherent High-Power THz Radiation On-Chip. *Phys. Rev. X* **7**, 041002 (2017).
- [12] Trocha, P. *et al.* Ultrafast optical ranging using microresonator soliton frequency combs. *Science* **359**, 887–891 (2018).
- [13] Suh, M.-G. & Vahala, K. J. Soliton microcomb range measurement. *Science* **359**, 884–887 (2018).
- [14] Spencer, D. T. *et al.* An optical-frequency synthesizer using integrated photonics. *Nature* **557**, 81–85 (2018).
- [15] Herr, T. *et al.* Temporal solitons in optical microresonators. *Nat. Photon.* **8**, 145–152 (2014).
- [16] Xue, X. *et al.* Mode-locked dark pulse Kerr combs in normal-dispersion microresonators. *Nat. Photon.* **9**, 594–600 (2015).
- [17] Savchenkov, A. A. *et al.* Low Threshold Optical Oscillations in a Whispering Gallery Mode CaF<sub>2</sub> Resonator. *Phys. Rev. Lett.* **93**, 243905 (2004).
- [18] Kippenberg, T. J., Spillane, S. M. & Vahala, K. J. Kerr-Nonlinearity Optical Parametric Oscillation in an Ultrahigh-Q Toroid Microcavity. *Phys. Rev. Lett.* **93**, 083904 (2004).
- [19] Li, J., Lee, H., Chen, T. & Vahala, K. J. Low-Pump-Power, Low-Phase-Noise, and Microwave to Millimeter-Wave Repetition Rate Operation in Microcombs. *Phys. Rev. Lett.* **109**, 233901 (2012).
- [20] Pu, M., Ottaviano, L., Semenova, E. & Yvind, K. Efficient frequency comb generation in AlGaAs-on-insulator. *Optica* **3**, 823–826 (2016).
- [21] Xuan, Y. *et al.* High-Q silicon nitride microresonators exhibiting low-power frequency comb initiation. *Optica* **3**, 1171–1180 (2016).
- [22] Ji, X. *et al.* Ultra-low-loss on-chip resonators with sub-milliwatt parametric oscillation threshold. *Optica* **4**, 619–624 (2017).
- [23] Bao, C. *et al.* Nonlinear conversion efficiency in Kerr frequency comb generation. *Opt. Lett.* **39**, 6126–6129 (2014).
- [24] Fülöp, A. *et al.* High-order coherent communications using mode-locked dark-pulse Kerr combs from microresonators. *Nat. Comm.* **9**, 1598 (2018).
- [25] Xue, X., Wang, P.-H., Xuan, Y., Qi, M. & Weiner, A. M. Microresonator Kerr frequency combs with high conversion efficiency. *Laser Photon. Rev.* **11**, 1600276 (2017).
- [26] Wang, P.-H. *et al.* Intracavity characterization of micro-comb generation in the single-soliton regime. *Opt. Exp.* **24**, 10890–10897 (2016).
- [27] Yu, M., Okawachi, Y., Griffith, A. G., Lipson, M. & Gaeta, A. L. Mode-locked mid-infrared frequency combs in a silicon microresonator. *Optica* **3**, 854–860 (2016).
- [28] Cole, D. C., Lamb, E. S., Del’Haye, P., Diddams, S. A. & Papp, S. B. Soliton crystals in Kerr resonators. *Nat. Photon.* **11**, 671–676 (2017).
- [29] Malinowski, M., Rao, A., Delfyett, P. & Fathpour, S. Optical frequency comb generation by pulsed pumping. *APL Photon.* **2**, 066101 (2017).

- [30] Obrzud, E., Lecomte, S. & Herr, T. Temporal solitons in microresonators driven by optical pulses. *Nat. Photon.* **11**, 600–607 (2017).
- [31] Xue, X., Zheng, X. & Weiner, A. M. Soliton trapping and comb self-referencing in a single microresonator with  $\chi^{(2)}$  and  $\chi^{(3)}$  nonlinearities. *Opt. Lett.* **42**, 4147–4150 (2017).
- [32] Liang, W. *et al.* Generation of a coherent near-infrared Kerr frequency comb in a monolithic microresonator with normal GVD. *Opt. Lett.* **39**, 2920–2923 (2014).
- [33] Lobanov, V. E., Lihachev, G., Kippenberg, T. J. & Gorodetsky, M. L. Frequency combs and platons in optical microresonators with normal GVD. *Opt. Exp.* **23**, 7713–7721 (2015).
- [34] Sample, A. P., Meyer, D. A. & Smith, J. R. Analysis, Experimental Results, and Range Adaptation of Magnetically Coupled Resonators for Wireless Power Transfer. *IEEE Trans. Ind. Electron.* **58**, 544–554 (2011).
- [35] Levy, J. S. *et al.* CMOS-compatible multiple-wavelength oscillator for on-chip optical interconnects. *Nat. Photon.* **4**, 37–40 (2010).
- [36] Herr, T. *et al.* Mode Spectrum and Temporal Soliton Formation in Optical Microresonators. *Phys. Rev. Lett.* **113**, 123901 (2014).
- [37] Xue, X. *et al.* Normal-dispersion microcombs enabled by controllable mode interactions. *Laser Photon. Rev.* **9**, L23–L28 (2015).
- [38] Bao, C. *et al.* Spatial mode-interaction induced single soliton generation in microresonators. *Optica* **4**, 1011–1015 (2017).
- [39] Xue, X., Zheng, X. & Zhou, B. Soliton regulation in microcavities induced by fundamental-second-harmonic mode coupling. arXiv:1804.02623.
- [40] Yi, X. *et al.* Single-mode dispersive waves and soliton microcomb dynamics. *Nat. Comm.* **8**, 14869 (2017).
- [41] Brasch, V. *et al.* Photonic chip-based optical frequency comb using soliton Cherenkov radiation. *Science* **351**, 357–360 (2016).
- [42] Xue, X. *et al.* Thermal tuning of Kerr frequency combs in silicon nitride microring resonators. *Opt. Exp.* **24**, 687–698 (2016).
- [43] Joshi, C. *et al.* Thermally controlled comb generation and soliton modelocking in microresonators. *Opt. Lett.* **41**, 2565–2568 (2016).
- [44] Jung, H., Fong, K. Y., Xiong, C. & Tang, H. X. Electrical tuning and switching of an optical frequency comb generated in aluminum nitride microring resonators. *Opt. Lett.* **39**, 84–87 (2014).
- [45] Hansson, T. & Wabnitz, S. Frequency comb generation beyond the Lugiato–Lefever equation: multi-stability and super cavity solitons. *J. Opt. Soc. Am. B* **32**, 1259–1266 (2015).
- [46] Anderson, M. *et al.* Coexistence of Multiple Nonlinear States in a Tristable Passive Kerr Resonator. *Phys. Rev. X* **7**, 031031 (2017).
- [47] Grudinin, I. S. *et al.* High-contrast Kerr frequency combs. *Optica* **4**, 434–437 (2017).
- [48] Miller, S. A. *et al.* Tunable frequency combs based on dual microring resonators. *Opt. Exp.* **23**, 21527–21540 (2015).
- [49] Agrawal, G. P. *Nonlinear Fiber Optics* (Academic Press, 2001).

# Supplementary information to Super-efficient temporal solitons in mutually coupled optical microresonators

Xiaoxiao Xue\*, Xiaoping Zheng, and Bingkun Zhou

*Department of Electronic Engineering, Beijing National Research Center for Information Science and Technology,  
Tsinghua University, Beijing 100084, China*  
[\\*xuexx@tsinghua.edu.cn](mailto:xuexx@tsinghua.edu.cn)

## 1. Energy transfer in coupled microresonators

The case of a single microresonator MR1 pumped by an incident field from port P is illustrated in Fig. S1a. The coupled-mode equations can be written as [S1]

$$\frac{dU_1}{dt} = (i\omega_1 - \kappa_P - \kappa_D)U_1 + \sqrt{2\kappa_P}a_P \quad (S1)$$

$$a_T = a_P - \sqrt{2\kappa_P}U_1 \quad (S2)$$

where  $U_1$  is the microresonator mode amplitude normalized so that  $|U_1|^2$  represents the energy;  $a_P$  and  $a_T$  are the field amplitudes at port P and port T, normalized so that  $|a_P|^2$  and  $|a_T|^2$  represent the power;  $\omega_1$  is the angular frequency of the microresonator;  $\kappa_P$  and  $\kappa_D$  are the coupling rates. The amplitude transfer function from port P to port T is given by

$$T(\omega_P) = \frac{a_T}{a_P} = 1 - \frac{2\kappa_P}{i(\omega_P - \omega_1) + \kappa_P + \kappa_D} \quad (S3)$$

where  $\omega_P$  is the pump angular frequency. When the pump frequency matches that of the microresonator ( $\omega_P = \omega_1$ ) and the coupling rates satisfy  $\kappa_P = \kappa_D$ , we have  $|T|=0$  which means the incident wave is completely absorbed by the microresonator and vanishes at port T. Based on energy conservation, it is easy to conclude that all the incident power from port P is dissipated to port D. When the pump frequency is detuned from the microresonator,  $|T|=0$  cannot be achieved which means full energy transfer is impossible.

If there is another microresonator MR2 (assumed intrinsically lossless) coupled to MR1 and the pump field, the coupled-mode equations become

$$\frac{dU_1}{dt} = (i\omega_1 - \kappa_D)U_1 + i\kappa_{12}U_2 \quad (S4)$$

$$\frac{dU_2}{dt} = (i\omega_2 - \kappa_P)U_2 + i\kappa_{21}U_1 + \sqrt{2\kappa_P}a_P \quad (S5)$$

$$a_T = a_P - \sqrt{2\kappa_P}U_2 \quad (S6)$$

where  $U_2$  and  $\omega_2$  are the mode amplitude and angular frequency of MR2; the coefficients of coupling between MR1 and MR2 obey the relation  $\kappa_{12} = \kappa_{21}^* = \kappa_C$ . The amplitude transfer function from port P to port T is given by

$$T(\omega_P) = \frac{a_T}{a_P} = 1 - \frac{2\kappa_P}{i(\omega_P - \omega_2) + \kappa_P + \frac{|\kappa_C|^2}{i(\omega_P - \omega_1) + \kappa_D}} \quad (S7)$$

Complete energy transfer from port P to port D can be achieved with  $|T| = 0$  when the following condition is satisfied

$$\kappa_P = \frac{|\kappa_C|^2 \kappa_D}{(\omega_P - \omega_1)^2 + \kappa_D^2} \quad (S8)$$

$$\omega_P - \omega_2 = \frac{|\kappa_C|^2 (\omega_P - \omega_1)}{(\omega_P - \omega_1)^2 + \kappa_D^2} \quad (S9)$$

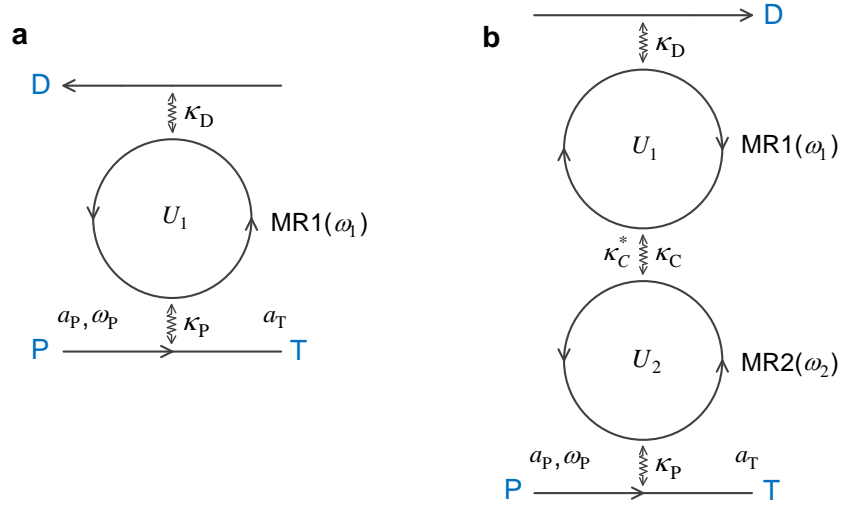


Figure S1 | Illustration of mode coupling in microresonators. (a) One single microresonator. (b) Two mutually coupled microresonators.

## 2. Derivation of the coupled nonlinear Schrödinger equations

We fold the dual coupled microring structure as in Fig S2b so that the propagation of the optical fields in MR1 and MR2 can be described with the same angular coordinate. The coupled nonlinear Schrödinger equations are written as [S2]

$$\begin{aligned} \frac{\partial E_1}{R_1 \partial \phi} = & \left[ -\alpha_{i1} + ik_1 - k_1' \frac{\partial}{\partial T} - i \frac{k_1''}{2} \frac{\partial^2}{\partial T^2} + i\gamma_1 |E_1|^2 \right] E_1 - \frac{1}{R_1} \sum_{n=-\infty}^{+\infty} \delta(\phi - n2\pi) (1 - \sqrt{1 - \theta_1}) E_1 \\ & + \frac{1}{R_1} \sum_{n=-\infty}^{+\infty} \delta(\phi - n2\pi - \pi) \left[ i\sqrt{\theta_{12}} E_2 - (1 - \sqrt{1 - \theta_{12}}) E_1 \right] \end{aligned} \quad (S10)$$

$$\begin{aligned} \frac{\partial E_2}{R_2 \partial \phi} = & \left[ -\alpha_{i2} + ik_2 - k_2' \frac{\partial}{\partial T} - i \frac{k_2''}{2} \frac{\partial^2}{\partial T^2} + i\gamma_2 |E_2|^2 \right] E_2 + \frac{1}{R_2} \sum_{n=-\infty}^{+\infty} \delta(\phi - n2\pi) \left[ i\sqrt{\theta_2} E_{in} - (1 - \sqrt{1 - \theta_2}) E_2 \right] \\ & + \frac{1}{R_2} \sum_{n=-\infty}^{+\infty} \delta(\phi - n2\pi - \pi) \left[ i\sqrt{\theta_{21}} E_1 - (1 - \sqrt{1 - \theta_{21}}) E_2 \right] \end{aligned} \quad (S11)$$

where  $\phi$  is the circular angle;  $T$  is the time (usually called fast time in the literature in contrast to a slow time corresponding to the propagation);  $R_{1,2}$  radii of MR1 and MR2;  $E_{1,2}$  the complex field amplitudes in MR1 and MR2, normalized so that  $|E_{1,2}|^2$  represent the power;  $E_{in}$  the pump field amplitude;  $\alpha_{i1,i2}$  the intrinsic amplitude loss per unit length;  $k_{1,2}$  the wave vectors;  $k_{1,2}' = dk_{1,2}/d\omega|_{\omega=\omega_p}$  reciprocal of the group velocities;  $k_{1,2}'' = d^2k_{1,2}/d\omega^2|_{\omega=\omega_p}$  group velocity dispersion;  $\gamma_{1,2}$  nonlinear coefficients;  $\theta_1$  power coupling ratio between MR1 and the drop waveguide;  $\theta_2$  power coupling ratio between MR2 and the pump waveguide;  $\theta_{12} = \theta_{21}$  power coupling ratio between MR1 and MR2;  $\delta(\bullet)$  the Dirac function.

Replace the variables  $\phi, T$  with  $z = R_1\phi, \tau = T - R_1\phi k_1'$ , the equations become

$$\begin{aligned} \frac{\partial E_1}{\partial z} = & \left[ -\alpha_{i1} + ik_1 - i \frac{k_1''}{2} \frac{\partial^2}{\partial \tau^2} + i\gamma_1 |E_1|^2 \right] E_1 - \sum_{n=-\infty}^{+\infty} \delta(z - nL) (1 - \sqrt{1 - \theta_1}) E_1 \\ & + \sum_{n=-\infty}^{+\infty} \delta\left(z - nL - \frac{L}{2}\right) \left[ i\sqrt{\theta_{12}} E_2 - (1 - \sqrt{1 - \theta_{12}}) E_1 \right] \end{aligned} \quad (S12)$$

$$\begin{aligned} \frac{\partial E_2}{\partial z} = & \left[ -\alpha_{i2}^s + ik_2^s - \Delta k^s \frac{\partial}{\partial \tau} - i \frac{k_2''^s}{2} \frac{\partial^2}{\partial \tau^2} + i\gamma_2^s |E_2|^2 \right] E_2 + \sum_{n=-\infty}^{+\infty} \delta(z - nL) \left[ i\sqrt{\theta_2} E_{in} - (1 - \sqrt{1 - \theta_2}) E_2 \right] \\ & + \sum_{n=-\infty}^{+\infty} \delta\left(z - nL - \frac{L}{2}\right) \left[ i\sqrt{\theta_{21}} E_1 - (1 - \sqrt{1 - \theta_{21}}) E_2 \right] \end{aligned} \quad (S13)$$

where  $z$  means the propagation distance in MR1;  $\alpha_{i2}^s, k_2^s, k_2''^s, \gamma_2^s$  are scaled parameters given by  $\alpha_{i2}^s = \alpha_{i2}R_2/R_1, k_2^s = k_2R_2/R_1, k_2''^s = k_2''R_2/R_1, \gamma_2^s = \gamma_2R_2/R_1$ ;  $\Delta k^s$  is the scaled group velocity mismatch given by  $\Delta k^s = k_2'R_2/R_1 - k_1'$ ;  $L = 2\pi R_1$  the round-trip length of MR1.

The round-trip phase delays can be written as  $k_1L = m_12\pi - \delta_{01}$  and  $k_2^sL = m_22\pi - \delta_{02}$ , where  $m_1, m_2$  are mode numbers of the microresonator modes that are pumped;  $\delta_{01}, \delta_{02}$  mean the round-trip phase detunings between the pump and the microresonator modes. Replace  $E_1$  and  $E_2$  with  $E_1' = E_1 e^{-ik_{m1}z}$  and  $E_2' = E_2 e^{-ik_{m2}z}$  where  $k_{m1}L = m_12\pi$  and  $k_{m2}L = m_22\pi$ , we have

$$\begin{aligned} \frac{\partial E_1'}{\partial z} = & \left[ -\alpha_{i1} - i\delta_1 - i\frac{k_1''}{2} \frac{\partial^2}{\partial \tau^2} + i\gamma_1 |E_1'|^2 \right] E_1' - \sum_{n=-\infty}^{+\infty} \delta(z-nL) (1-\sqrt{1-\theta_1}) E_1' \\ & + \sum_{n=-\infty}^{+\infty} \delta\left(z-nL-\frac{L}{2}\right) \left[ i\sqrt{\theta_{12}} E_2' e^{i(m_2-m_1)\pi} - (1-\sqrt{1-\theta_{12}}) E_1' \right] \end{aligned} \quad (\text{S14})$$

$$\begin{aligned} \frac{\partial E_2'}{\partial z} = & \left[ -\alpha_{i2}^s - i\delta_2 - \Delta k^s \frac{\partial}{\partial \tau} - i\frac{k_2''}{2} \frac{\partial^2}{\partial \tau^2} + i\gamma_2^s |E_2'|^2 \right] E_2' + \sum_{n=-\infty}^{+\infty} \delta(z-nL) \left[ i\sqrt{\theta_2} E_{\text{in}} - (1-\sqrt{1-\theta_2}) E_2' \right] \\ & + \sum_{n=-\infty}^{+\infty} \delta\left(z-nL-\frac{L}{2}\right) \left[ i\sqrt{\theta_{21}} E_1' e^{i(m_1-m_2)\pi} - (1-\sqrt{1-\theta_{21}}) E_2' \right] \end{aligned} \quad (\text{S15})$$

where  $\delta_1 = \delta_{01}/L$  and  $\delta_2 = \delta_{02}/L$  the averaged phase detunings.

When  $|m_1 - m_2|$  is even, the related phase terms in Eqs. (S14) and (S15) are just 1. When  $|m_1 - m_2|$  is odd, the phase terms are  $-1$  meaning that there is a  $\pi$  phase difference between  $E_1'$  and  $E_2'$  at the MR1-MR2 coupling point. In this case, we can do a further variable replacement with  $E_1' = -E_1''$ , then we arrive at the same form of equations as when  $|m_1 - m_2|$  is even. To simplify the denotations, we still use  $E_1, E_2$  to represent  $E_1'$  (or  $E_1''$ ),  $E_2'$ ; and  $\alpha_{i2}, \Delta k^s, k_2'', \gamma_2^s$  to represent the scaled parameters  $\alpha_{i2}^s, \Delta k^s, k_2'', \gamma_2^s$ . Finally we have the following set of equations describing the field evolution in MR1 and MR2, together with those for the fields in the bus waveguides.

$$\begin{aligned} \frac{\partial E_1}{\partial z} = & \left[ -\alpha_{i1} - i\delta_1 - i\frac{k_1''}{2} \frac{\partial^2}{\partial \tau^2} + i\gamma_1 |E_1|^2 \right] E_1 - \sum_{n=-\infty}^{+\infty} \delta(z-nL) (1-\sqrt{1-\theta_1}) E_1 \\ & + \sum_{n=-\infty}^{+\infty} \delta\left(z-nL-\frac{L}{2}\right) \left[ i\sqrt{\theta_{12}} E_2 - (1-\sqrt{1-\theta_{12}}) E_1 \right] \end{aligned} \quad (\text{S16})$$

$$\begin{aligned} \frac{\partial E_2}{\partial z} = & \left[ -\alpha_{i2} - i\delta_2 - \Delta k^s \frac{\partial}{\partial \tau} - i\frac{k_2''}{2} \frac{\partial^2}{\partial \tau^2} + i\gamma_2 |E_2|^2 \right] E_2 + \sum_{n=-\infty}^{+\infty} \delta(z-nL) \left[ i\sqrt{\theta_2} E_{\text{in}} - (1-\sqrt{1-\theta_2}) E_2 \right] \\ & + \sum_{n=-\infty}^{+\infty} \delta\left(z-nL-\frac{L}{2}\right) \left[ i\sqrt{\theta_{21}} E_1 - (1-\sqrt{1-\theta_{21}}) E_2 \right] \end{aligned} \quad (\text{S17})$$

$$E_T = i\sqrt{\theta_2} E_2|_{z=nL} + \sqrt{1-\theta_2} E_{\text{in}} \quad (\text{S18})$$

$$E_D = i\sqrt{\theta_1} E_1|_{z=nL} \quad (\text{S19})$$

where  $E_T$  and  $E_D$  denote the complex field amplitudes at port T and D.



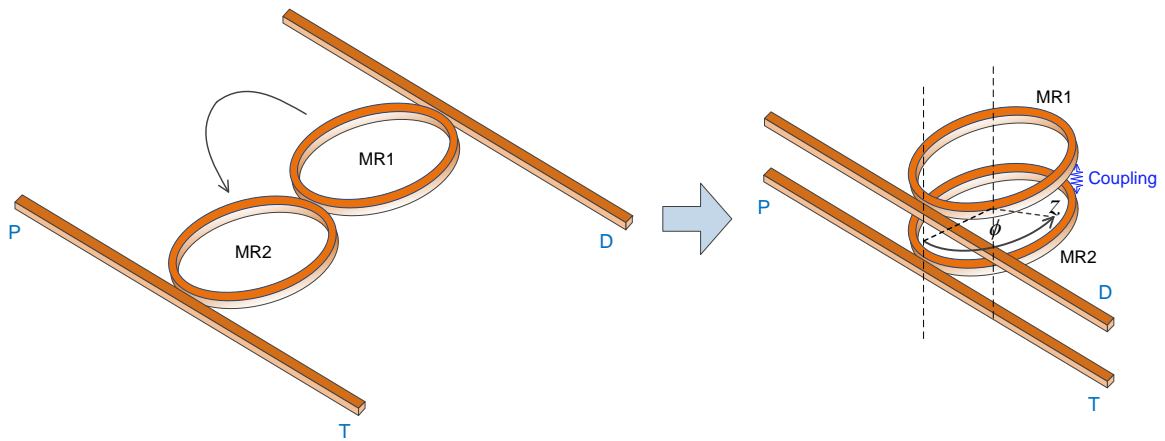


Figure S2 | Illustration of folding the mutually coupled microresonators for equation derivation.

## References

- [S1] Vahala, K. *Optical Microcavities* (World Scientific, 2004).
- [S2] Agrawal, G. P. *Nonlinear Fiber Optics* (Academic Press, 2001).